

Self-Assemblies of Zinc Complexes for Aggregation-Induced Emission Luminogen Precursors

Rinki Brahma and Jubaraj B. Baruah*



Cite This: *ACS Omega* 2020, 5, 3774–3785



Read Online

ACCESS |



Metrics & More

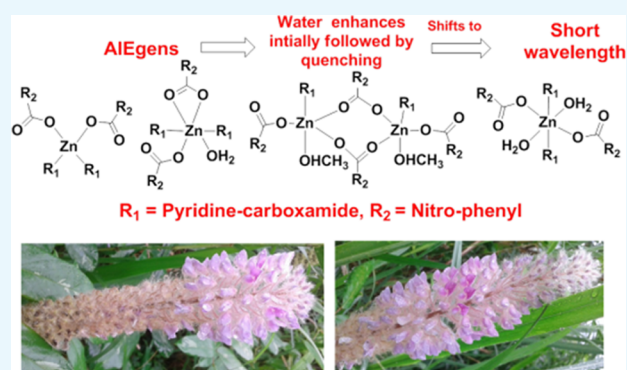


Article Recommendations



Supporting Information

ABSTRACT: Positional isomers of zinc–nitrobenzoate complexes possessing pyridine -3-(or-4-) carboxamide are used for a comparative theoretical and experimental study to understand their utility as model complexes to understand the role of metal-to-ligand charge transfer in aggregation-induced emission (AIE). Among the five different model zinc complexes, four of them are non-ionic, and one is an ionic complex. The frontier molecular energy levels of different combinations of the positional isomeric complexes and the absorption maximum were ascertained by density functional theory calculations. The PolyQ value obtained from solid samples of each complex is different. Shifts in the emissions to higher wavelengths than the expected emission for the S_1 to S_0 transition were observed due to aggregations. The highest value of PolyQ among the complexes was 13.56% observed for emission at 439 nm ($\lambda_{ex} = 350$) of the non-ionic complex, namely, (di-aqua)bis(pyridine-3-carboxamide)di(2-nitrobenzoato)zinc(II) monohydrate. Close resemblance in emission lifetime decay profiles of the solid samples of those complexes and the respective solutions of those complexes in dimethyl sulfoxide with or without water showed a common trend, suggesting aggregation-induced emission in each case. Aggregation-induced emission caused by adding water in dimethyl sulfoxide solution of each complex showed an initial increase without a shift in the emission wavelength followed by a quenching with a shift of the respective emission peak to a short wavelength. Dynamic light scattering studies showed an increase in the average particle sizes upon an increase in the concentration of water. This indicated initial participation of water molecules to form aggregates with the complexes, favoring an increase in the AIE intensity. Aggregation of each complex changes with the concentration of water, and an increase in the concentration of water beyond a characteristic limit causes lowering of the emission intensity to the short wavelength.



INTRODUCTION

The self-assembly of various zinc complexes shows novel emission properties.^{1–8} Many zinc complexes have prospects as applied optoelectronic materials.^{9–11} Besides enhanced chemical reactivity for catalytic reactions,^{12–18} optoelectronic properties of zinc oxide necessitate the study of polynuclear zinc clusters possessing a ZnO_4 environment.^{19–25} Solvent plays an important role in the synthesis of such zinc clusters or coordination polymers.^{26,27} Design of ligands^{28–33} and improvisation of noncovalent interactions of ligands are common ways to synthesize complexes with less conventional coordination numbers such as five-coordinated^{34,35} zinc complexes. A careful look at the number of zinc complexes suggests that, irrespective of ligands, they show emissions near 400–430 nm with some exceptions.^{1–8} Some d^{10} zinc complexes show sample- and size-dependent fluorescence emissions,³⁶ whereas in certain cases, aggregation-induced emissions (AIE) of zinc complexes are comparable to similar emissions by corresponding d^{10} cadmium complexes.³⁷ Those observations together with the emergence of AIEgens of zinc complexes^{38–41} and the development of newer aspects of

AIEgens^{42,43} make one curious to explore the emission behavior of simple zinc complexes. Furthermore, the AIEgens are generally developed from fluorescent compounds, whereas a metal complex helps to bring together nonfluorescent components to modulate emission based on metal-to-ligand charge-transfer transitions. In such cases, d^{10} electronic configuration is of a special interest, as it contributes to the emission through charge-transfer transition.^{38–41} Hence, there is a necessity to look at the emissions of representative zinc complexes of different independent structures. It would be imperative to bring about significant structural variations with a minimal change on the ligands to understand the effect of aggregation of those complexes in their respective emissive properties. Hence, we have undertaken this study on zinc complexes derived from binary combinations of the positional

Received: January 11, 2020

Accepted: January 29, 2020

Published: February 12, 2020



isomers of nitrobenzoic acid and pyridinecarboxamide shown in Figure 1. The objective is to examine different types of

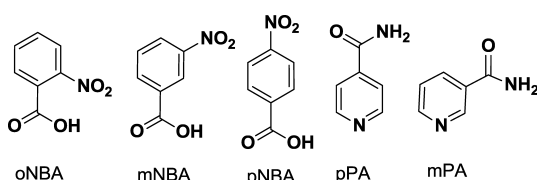
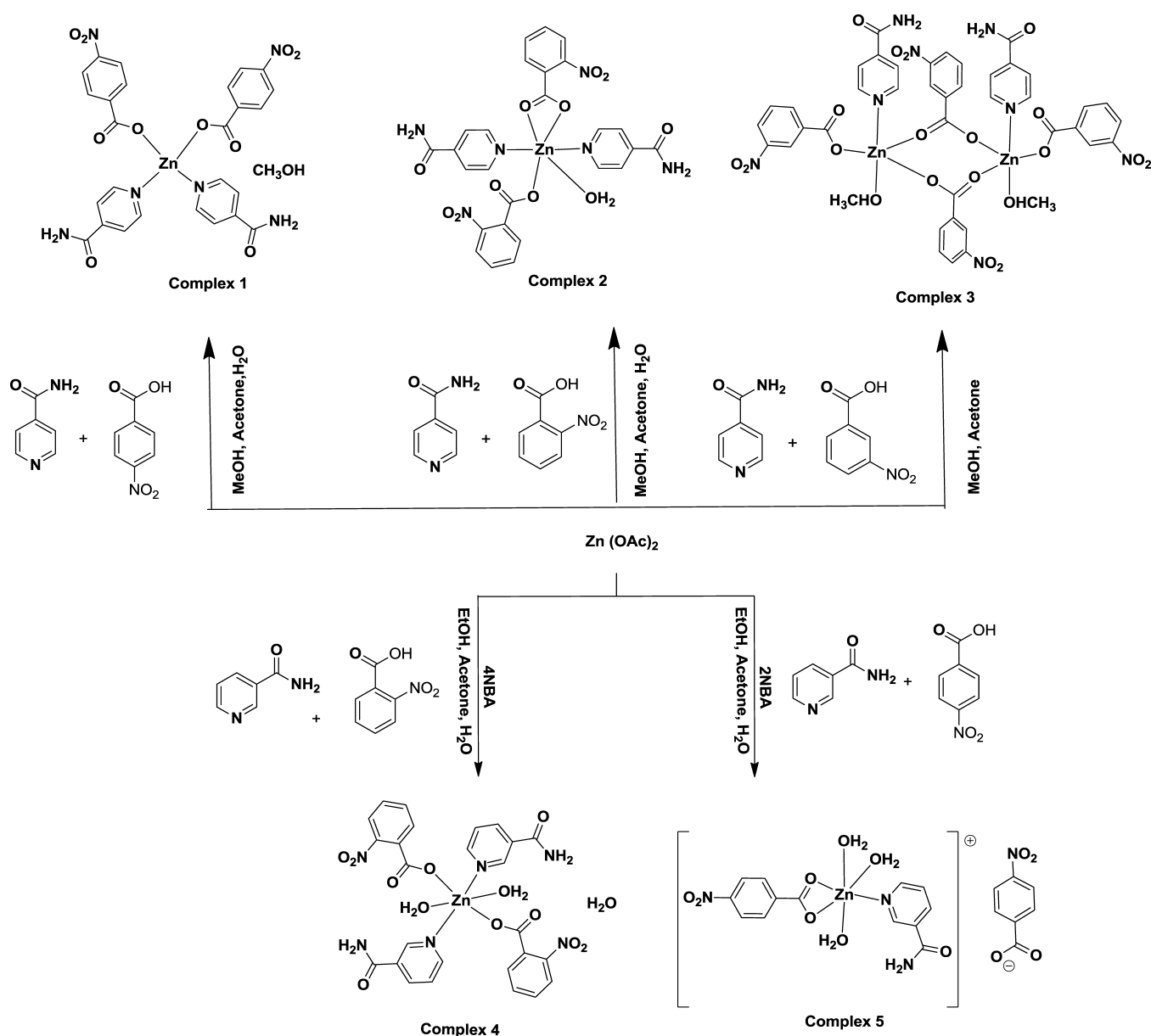


Figure 1. Positional isomers of nitrobenzoic acid and pyridinecarboxamide used for complexation with zinc ion in this study.

structures and their self-assembly in solid and solution to unearth aggregation-induced emissions.^{44–46} The preliminary issues to be addressed are (i) characterization of structures and self-assemblies of the zinc complexes derived from positional isomeric ligands, (ii) theoretically formulating the relative stabilities and the frontier orbitals of new structures formulated

based on the experimentally observed structures, and (iii) understanding those complexes as precursors for AIE luminogens (AIEgens). In the quest to obtain answers to these issues, we have taken up a study on structural and theoretical aspects as well as emission properties of five zinc complexes shown in Scheme 1. The choices of the ligands are based on the facts that the zinc–nitrobenzoate complexes^{47,48} are well known to show structural varieties and the amide functional group can provide hydrogen-bonding sites for the formation of directional self-assemblies. Depending on the structure and the composition of an ionic or a non-ionic d^{10} zinc(II) complex, the electronic and steric factor would provide different impacts on emission properties, whereas an amide group of a ligand would provide sites for the formation of hydrogen bonds. The presence of an amide-containing ligand together with a carboxylate ligand in a metal complex of such kinds would enhance self-assembly required for an aggregation-induced emission.

Scheme 1. Synthesis of Different Positional Isomeric Zinc–Nitrobenzoate Complexes



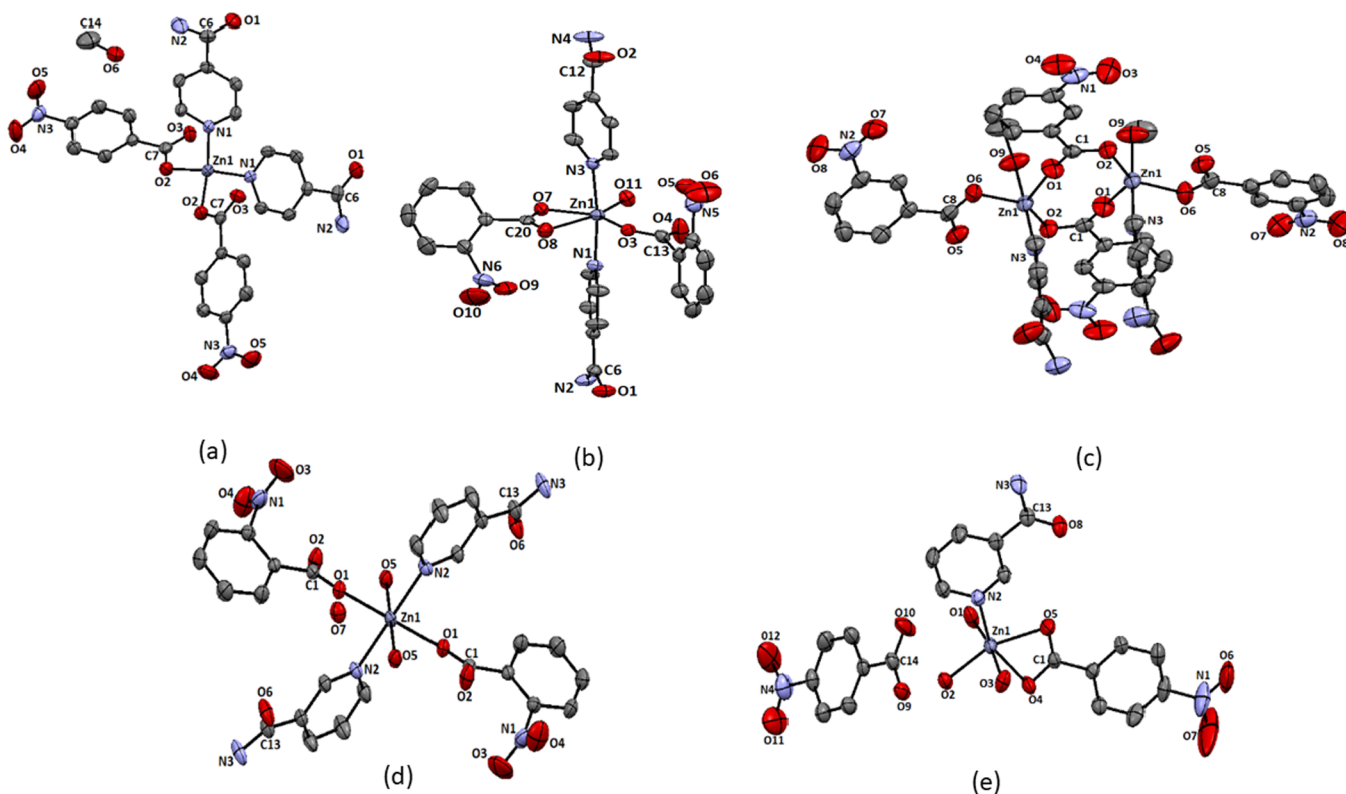


Figure 2. Structure of complexes (a) 1, (b) 2, (c) 3, (d) 4, and (e) 5 (drawn with 50% thermal ellipsoids).

RESULTS AND DISCUSSION

Synthesis and Characterization of Zinc Complexes.

The reactions of positional isomers of nitrobenzoic acid together with pyridine-4-carboxamide amide and zinc(II) acetate under ambient conditions resulted in the formation of three different non-ionic zinc complexes (Scheme 1). A similar reaction of 2-nitrobenzoic acid and pyridine-3-carboxamide with zinc(II) acetate provided a non-ionic complex, whereas a reaction of 4-nitrobenzoic acid and pyridine-3-carboxamide with zinc(II) acetate yielded an ionic complex. We could not obtain a crystalline product from the reaction of 3-nitrobenzoic acid and pyridine-3-carboxamide with zinc(II) acetate. Each isolated complex was structurally characterized by single-crystal X-ray crystallography and powder X-ray diffraction (XRD) (Figure S1), ^1H NMR (Figures S2–S6), and ^{13}C NMR spectroscopy (Figures S7–S10). Attempts to prepare the complex in other compositions by varying the stoichiometry of the reactants were not successful. The phase purity of each complex was determined by recording their respective powder XRD pattern and comparing those patterns with the powder XRD pattern generated from the respective CIF file. The literature suggests wide structural variations in isonicotimide-containing zinc complexes depending on the partner carboxylic acid;^{47,49} in certain cases, dinuclear complexes were observed.⁵⁰

The complex bis(pyridine-4-carboxamide)di(4-nitrobenzoato)zinc(II)-methanol (1) is a mononuclear complex with tetrahedral geometry (Figure 2a). The complex has two pyridine-4-carboxamide molecules as N-donor ligands and two monodentate 4-nitrobenzoates to provide a N_2O_2 environment to the central zinc ion. The complex is devoid of a coordinating solvent, but it has a methanol molecule as a solvent of crystallization. The structure of the complex is

shown in Figure 2a; it has a symmetric structure where each pair of identical ligands is related by a mirror plane. The Zn1–N1 bond distance is 2.032(2) Å, and the Zn1–O2 bond distance is 1.951(18) Å. The ^1H NMR spectra of the complex show signals for the protons of the two aromatic ligands. Each has AA'BB' patterns, which are expected to appear at four independent chemical shift positions, but these are observed as three sets of protons. The proton signal appearing as broad unresolved peaks at 7.77 ppm are from the nitrobenzoate ring. The AA'BB' pattern observed at 8.27 and 8.15 ppm are from the hydrogen atoms of pyridine-4-carboxamide. This is also supported by the corresponding integration of the proton signals at those chemical shift positions (refer to Supporting Figure S2). The amide protons appear as a broad peak at 8.74 ppm; broad nature suggests a slow exchange of hydrogen atoms of the amide group with water molecules present in the solvent. The IR spectra of the complex has a 1408 cm^{-1} sharp peak due to the nitro group. It shows broad peaks at 3443 cm^{-1} for the O–H of the solvent and 3370 and 3156 cm^{-1} for stretching due to hydrogen-bonded N–H bond of the amide group.

The six-coordinate complex bis(pyridine-4-carboxamide)-(aqua)di(2-nitrobenzoato)zinc(II) (2) with two pyridine-4-carboxamide molecules at *trans* positions was obtained from the reaction of zinc acetate with pyridine-4-carboxamide and 2-nitrobenzoic acid. This structure is not unusual and come across in similar combination with a cobalt analogue reported earlier.⁵¹ There are also ample examples of complexes based on nitrobenzoate and nicotinamide ligands with first row transition metal ions to suggest that structures of those complexes varies with the central metal ion.^{52,53} Among, the two carboxylates coordinating to zinc ion in the complex, one carboxylate is monodentate, and the other is bis-chelating. A

water molecule occupies the sixth coordination site. The two Zn–N bonds are 2.166(4) and 2.188(3) Å, whereas the three Zn–O_{carboxy} bonds are 2.013(2), 2.151(2), and 2.409(3) Å, respectively (Figure 2b). The relatively large Zn1–O8 bond shows that the carboxylate is not chelating to the zinc ion in a symmetric manner; an oxygen atom is very weakly bound to the zinc ion with respect to the other ligating oxygen atom. On the other hand, the Zn–O_{aqua} bond distance is 2.032(3) Å, which is indicative of having a tightly bound water molecule in the complex. The complex shows complementing intermolecular hydrogen bonds between the amides. ¹H NMR of the complex has signals for the protons of pyridine-4-carboxamide at 7.76 and 8.70 ppm, whereas 2-nitrobenzoate shows peaks at 7.57 and 7.65 ppm, and other peaks overlap with the ring protons of pyridine-4-carboxamide appearing at 7.76 ppm. The NH₂ protons appear at 8.31 ppm as a sharp peak. The compound shows characteristic NO₂ stretching signals at 1523 and 1384 cm⁻¹. The O–H and N–H stretching is observed as a broad and sharp peak at 3392 cm⁻¹. The two peaks at 1690 and 1523 cm⁻¹ are assigned to amide I and amide II stretching, respectively. The signal at 1613 cm⁻¹ is due to carboxylate stretching.

In contrast to these, the zinc-3-nitrobenzoate complex with pyridine-4-carboxamide is a dinuclear complex. The complex di- μ^2 -(3-nitrobenzoato)[(methanol)(pyridine-3-carboxamide)-(3-nitrobenzoato)zinc(II)] (3) has two equivalent zinc ions, each possesses one pyridine-4-carboxamide, a methanol molecule, and a bis-chelated 3-nitrobenzoate ligand to form one site, and two such sites are bridged through two carboxylate bridges offered by two 3-nitrobenzoates, which provide the skeleton of the binuclear complex. The interesting feature of the complex is that each zinc site is pentacoordinated with slightly distorted trigonal-bipyramidal geometry (Figure 2c). The geometry around each metal ion is a distorted trigonal bipyramid. This geometry is reflected in the bond angles forming the trigonal plane. Namely, these bond angles are 124.8(8)° (\angle O1–Zn1–O2), 92.9(9)° (\angle O1–Zn1–O6), and 141.7(8)° (\angle O2–Zn1–O6), whereas the bond angle between the two axial bonds is 177.27(8)° (\angle O9–Zn1–N3). The Zn1–O1, Zn1–O2, Zn1–O6, and Zn1–O9 bond distances are 2.022(2), 2.024(2), 2.036(2), and 2.090(2) Å, respectively, whereas the Zn1–N3 bond distance is 2.134(2) Å. These are in the range of conventional zinc–oxygen and zinc–nitrogen complex found in zinc carboxylate complexes. Generally, paddle-wheel structures, μ^2 -bridging mode⁵⁴ of carboxylate alone or together with side-on μ^1 -bridging mode,⁵⁵ are observed in zinc carboxylate complexes. In the present case, complex 3 has two bridging carboxylates and two monodentate carboxylates. Such a bonding scheme provides an unconventional structure and geometry, leaving scopes for further transformations of such a backbone. In solution, the ¹H NMR spectra of the complex do not distinguish the bridging and terminal 3-nitrobenzoate ligands. This is possibly due to a fast exchange, which is not noticed at the NMR time scale. There are signals at 7.77 and 8.31 ppm for the ring protons of pyridine-4-carboxamide. The amide protons appear at 8.66 ppm, whereas the ring protons of 3-nitrobenzoate are observed at 8.29, 8.35, and 7.71 ppm. The coordinated methanol gives peaks at 4.21 ppm for O–H and at 3.16 ppm for methoxy protons. There are two peaks in ¹³C NMR for carbonyl carbons of the amide and carboxylic acid at 169.34 and 166.67 ppm, respectively. The signal for the bridging methanol molecules of the complex is observed as one peak at 48.92

ppm. These point out the symmetric nature of the complex existing in solution. The complex shows IR absorption for O–H of methanol at 3582 cm⁻¹; the N–H stretching and amide I and amide II bands of amides appear at 3317, 1687, and 1561 cm⁻¹, respectively, whereas there is stretching at 1612 cm⁻¹ due to carboxylate. The absorption due to the nitro group stretching is observed at 1525 and 1475 cm⁻¹. No clear distinctions on bridging and terminal carboxylate could be seen from the solid-state IR spectra also.

The activation energy to form a chelate from a monodentate carboxylate is about 6 kJ/mol.⁵⁶ This small barrier enables metal–carboxylate complexes to adopt varieties of structures upon slight variations on the ligands and reaction conditions. Thus, pyridine-3-carboxamide, which is another positional isomer, was used to prepare similar zinc complexes. We found large differences in the compositions and structures of the complexes from the complexes of pyridine-4-carboxamide. Namely, the complex prepared from a combination of pyridine-3-carboxamide and 2-nitrobenzoic acid reacting with zinc(II) acetate provided (di-aqua)bis(pyridine-3-carboxamide)di(2-nitrobenzoato)zinc(II) monohydrate (4). This hexacoordinated complex has an octahedral geometry. It has two water molecules at the axial positions *trans* to each other, whereas the 2-nitrobenzoates and pyridine-3-carboxamide molecules occupy the basal plane of the distorted octahedral geometry. The ligands of same kinds occupy *trans* positions. The Zn–O_{carboxy}, Zn–O_{aqua}, and Zn–N bond distances are 2.184(12), 2.120(13), and 2.145(15) Å, respectively (Figure 2d). The 1:1 ratio of the two ligands is reflected in the integration of the ¹H NMR spectra of the complex. The protons of the pyridine-3-carboxamide ring appear at 9.02, 8.70, and 7.79 ppm. The amide peak appears as multiplet peak at 8.16–8.21 ppm, suggesting an independent environment for two amides. The O–H stretching and amide stretching of the complex are observed at 3388 and 3154 cm⁻¹, whereas the amide I and amide II bands are observed at 1681 and 1601 cm⁻¹, respectively. Nitro stretching is observed at 1534 and 1440 cm⁻¹.

Finally, the complex [triaqua(pyridine-3-carboxamide)(κ -O- κ -O'-4-nitrobenzoato)zinc(II)]4-nitrobenzoate (5) is an exception among the five complexes as it is obtained as an ionic complex. The ratio of pyridine-3-carboxamide in complexes 4 and 5 is different. Complex 5 has one 4-nitrobenzoate as a chelating ligand, and it also has a 4-nitrobenzoate anion outside the coordination sphere. The complex has one pyridine-3-carboxamide molecule as the N-donor ligand, and there are three water molecules coordinating to zinc ions. The three water molecules in the coordination sphere are meridional. The carboxylate chelate is almost symmetric, and the two Zn–O_{carboxy} bond distances are 2.167(3) and 2.188(3) Å (Figure 2e). The two water molecules are tightly bound to the zinc ion, where Zn–O_{aqua} distances are 2.089(4) and 2.011(3) Å, whereas the third water molecule is weakly bound, and it has a zinc–oxygen bond distance of 2.204(3) Å. The zinc–nitrogen bond distance is 2.056(4) Å. The 4-nitrobenzoate group shows AA'BB' signals for pyridine-3-carboxamide at 8.26 and 8.16 ppm. The ¹H NMR signals however do not distinguish the anionic or ligating nitrobenzoate. This complex also shows the two CH signals at 9.03 and 8.70 ppm. The ¹³C NMR spectra of the complex have two ¹³C signals for C=O at 169.60 and 166.76 ppm, suggesting only one complex in solution. The IR spectra shows OH stretching at 3556 cm⁻¹, amide N–H at 3428–3115 cm⁻¹,

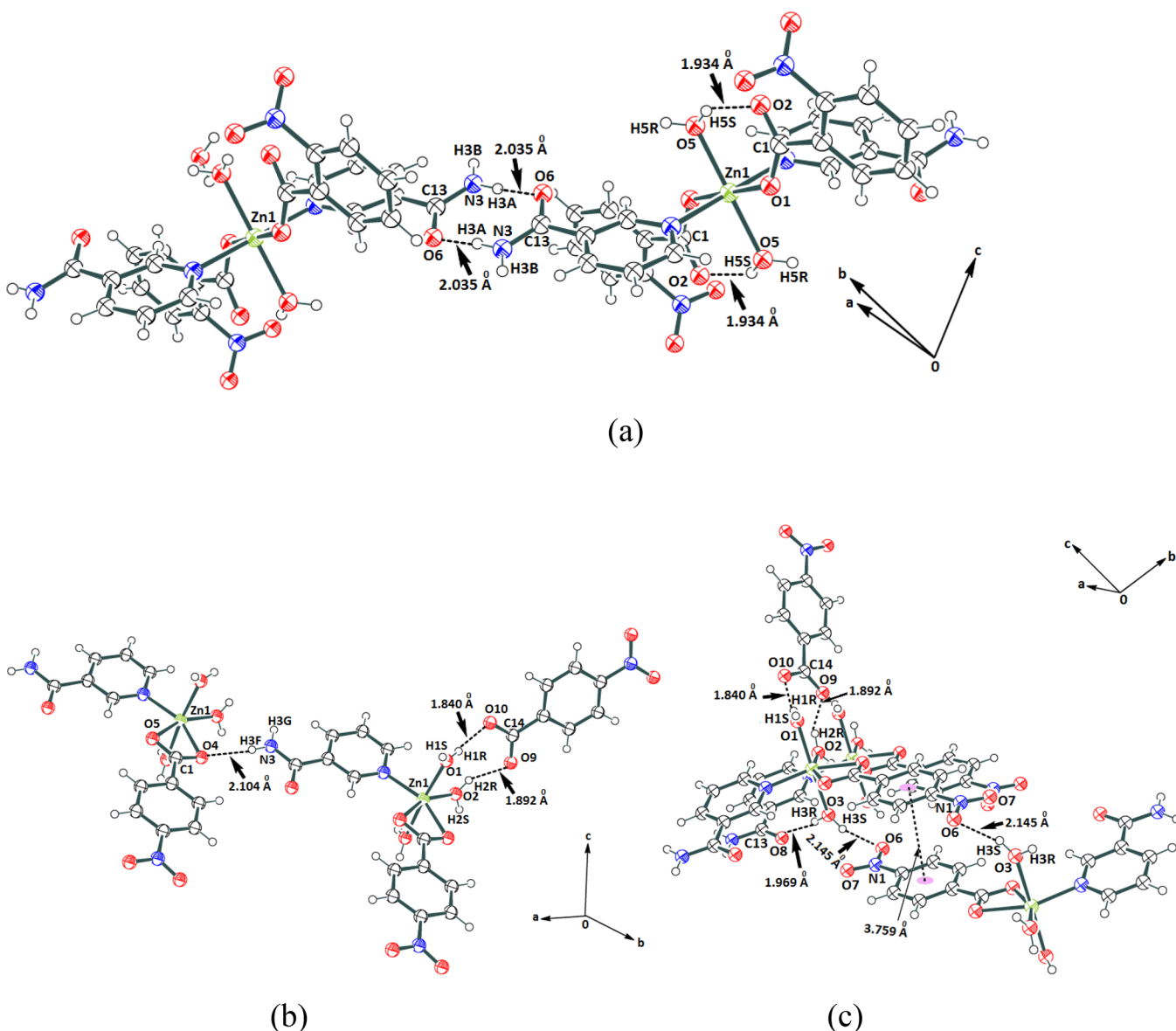


Figure 3. (a) Hydrogen-bonded self-assembly of (a) complex 4. (b, c) Hydrogen-bonded assembly of complex 5 viewed from two different directions.

amide I at 1680 cm^{-1} , and amide II band at 1609 cm^{-1} . The nitro groups show characteristic absorptions at 1558 and 1427 cm^{-1} . Furthermore, the complex 5 is an ionic complex in contrast to all other non-ionic complexes observed in this study. The fundamental differences between these two complexes 4 and 5 are in the coordination numbers, geometries, numbers of pyridinecarboxamide ligand per zinc ion, the binding behavior of the carboxylates, and the water of crystallization.

Each complex is self-associated through hydrogen bonds. The self-assemblies of the complexes 1–3 are shown in Supporting Figure S11–S13. There are interesting aspects on hydrogen bonds in the self-assemblies of complexes 4 and 5. The self-assembly of complex 4 has intramolecular hydrogen bonds involving the coordinated water molecule (Figure 3a). The amide–amide hydrogen bonds are prominent in the self-assembly. The water of crystallization molecules has a role in the formation of self-assembly of complex 4. The oxygen atoms of neighboring carboxylates of the nitrobenzoate ligands are

intermolecularly linked through hydrogen-bonded bridges offered by the water molecule of crystallization, whereas complex 5 has two water molecules occupying *cis* positions, which form complementary charge-assisted hydrogen bonds of cyclic synthons (Figure 3b). The third water molecule on the complex forms hydrogen bonds with an oxygen atom of a nitro group and an oxygen atom of an amide group of two independent molecules of the complex (Figure 3c). The hydrogen-bond parameters are listed in Supporting Table S3.

Fluorescence Emission of the Complexes. There are scopes to understand the mechanistic aspects of the emission properties of discrete and self-assemblies of zinc complexes.^{57–60} Complexes 1–5 in the solid state are weakly fluorescent and emit around 434 – 463 nm upon excitation at 350 nm (Figure 4). The observed emissions are similar to the one observed from the aggregation-induced emissions from self-assemblies of zinc complexes.⁶¹ Theoretical calculations based on density functional theory (DFT) using the B3LYP functional with LANL2DZ as a basis set have suggested that

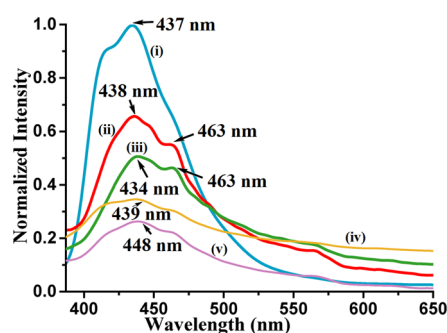


Figure 4. Fluorescence emission of the solid sample of (i) complex 2 ($\lambda_{em} = 437$ nm), (ii) complex 3 ($\lambda_{em} = 438, 463$ nm), (iii) complex 1 ($\lambda_{em} = 434, 463$ nm), (iv) complex 4 ($\lambda_{em} = 439$ nm), and (v) complex 5 ($\lambda_{em} = 448$ nm) ($\lambda_{ex} = 350$ nm in all cases).

HOMO–LUMO gaps for complexes 1–4 as 299.72, 334.22, 328.01, and 317.13 nm, respectively. Further to these, TD-DFT calculations performed have predicted that the absorptions of complexes 1–5 are at 340, 383, 332, 392, and 326 nm, respectively (Table 1).

Thus, the experimentally observed emissions are at much longer wavelengths than those theoretically expected S_1 to S_0 transitions. The emissions observed at a higher wavelength in the solid state as compared to theoretical gaps suggest an aggregation-induced emission. The PolyQ value for all the complexes were determined varied between 0.56 and 13.56% are listed in Table S2. Among the complexes, complex 4 has the highest quantum yield, whereas ionic complex 5 has the least quantum yield. The rates of radiative and non-radiative emission paths are calculated and listed in Table 1. The radiative transitions are indicative of closely associated multiple energy levels to have decayed through energy dissipation, which points toward an aggregation-induced emission.

The relative magnitude of the quantum yields (PolyQ) are in the order complex 4 > complex 2 > complex 3 > complex 1 > complex 5. Complex 5 is weakly fluorescent with a quantum yield of 0.56%; relative to complex 5, complex 4 has 21.4 times higher PolyQ, whereas complex 3 has 7.4 times higher PolyQ than complex 5. The PolyQ value of the solid sample of complex 3 is comparable to complex 1. The lifetime decay profile of each complex shows biexponential decay. Among the two lifetimes observed in each case, a higher fraction of molecules (approximately 60% in each case) follows a relatively shorter decay path having a lifetime in range of 0.558–0.848 ns. The rest of the excited molecules follows another path that has lifetimes in the range of 3.025–4.553 ns. In earlier lifetime studies on zinc–salen complexes, the biexponential lifetime was observed in solid samples, which

was suggested to arise from different orientations of self-assembled molecules in the unit cell.⁵⁹ The observed emissions are aggregation-induced as the emissions occur at relatively higher wavelengths than those expected from theoretically calculated HOMO–LUMO gaps, and also the emission decay profiles are similar. Relative intensities of the shoulder on the principal emission peak in each case differ from each other. The shoulders of the principal peaks are attributed to different fast exchanging assemblies. Hence, the overall change in the intensity of the respective complex is due to change in the coordination contributing to facilitate or modify the domains in each assembly to influence the transition probabilities and wavelength of emission. There are a large number of AIEgens in which there is an initial increase in emission intensity followed by quenching.^{59–61} In well-defined assemblies of resorcin-4-calixarene dissolved in a chloroform–water mixture, the distribution of water molecules in an internal and external periphery of the self-assembled structure is distinguishable at different concentrations.⁶² The emission spectra of complexes 1–5 in dimethyl sulfoxide (DMSO) solution show aggregation-induced emissions (Figure 5). In each case, the prominent emission is at a wavelength varying from 396 to 441 nm. The emission in each case initially increases followed by quenching upon addition of water, and the profiles are shown in Figure 4. Complex 3 has emissions at 412 and 431 nm and a shoulder at 397 nm, and the intensities of emissions are enhanced when the solution contains 10% water; after this concentration, there is a continuous decrease in the emission, and the emission peak positions change to show a distinct low-intensity emission peak in the wavelength that range between 380 and 397 nm. The changes are attributed to initial water-assisted aggregation, which, upon progressive addition of water, breaks down to show the emission of monomeric species. On the other hand, complex 4 shows an increase in emission at 416 nm till 10% water, and then emission intensity is reduced; while quenching, it shifts to 397 nm. Similarly, complex 5 shows enhancement of emissions at 396, 417, and 441 nm until 30% water content in solution; beyond this, there is a decreasing trend in emission intensities upon further increase in the percentage of water.

In this case, there is a very small shift in the position of emission. Hence, a change in aggregation followed by the formation of a compartmentalized aggregate or segregation of aggregate is taking place. Similar trends are observed from other complexes, supporting a similar mechanism operative upon addition of water in each case. It may be noted that the aggregation-induced emissions are reported of zinc complexes with fluorescence-active ligands.^{38–41} However, in the present study, the ligands are nonfluorescent. The quantum yield of each complex in DMSO is very low, yet they provide enough

Table 1. Quantum Yield, Lifetime of the Excited State, Rate Constant of Nonradiative and Radiative Decay of Solid Samples, and TD-DFT Calculated Absorption Maxima and Oscillator Strengths

complex	observed emission wavelength (nm)	quantum yield (Φ_F) ^a	lifetime for the excited state, τ (ns)	k_{nr} (10^7 s ⁻¹)	k_r (10^7 s ⁻¹)	TD-DFT calculated	
						λ_{max} (nm)	oscillator strength (f)
1	437	0.0414	3.788	25.30	1.093	340	0.0003
2	438	0.0261	3.554	27.40	0.734	383	0.0095
3	434	0.0148	3.025	32.57	0.489	332	0.0002
4	439	0.1356	3.506	24.65	3.867	392	0.0350
5	448	0.0056	3.780	26.30	0.148	326	0.0149

^aIn each case, biexponential decay is observed, and only the higher lifetime relating AIE is shown here.

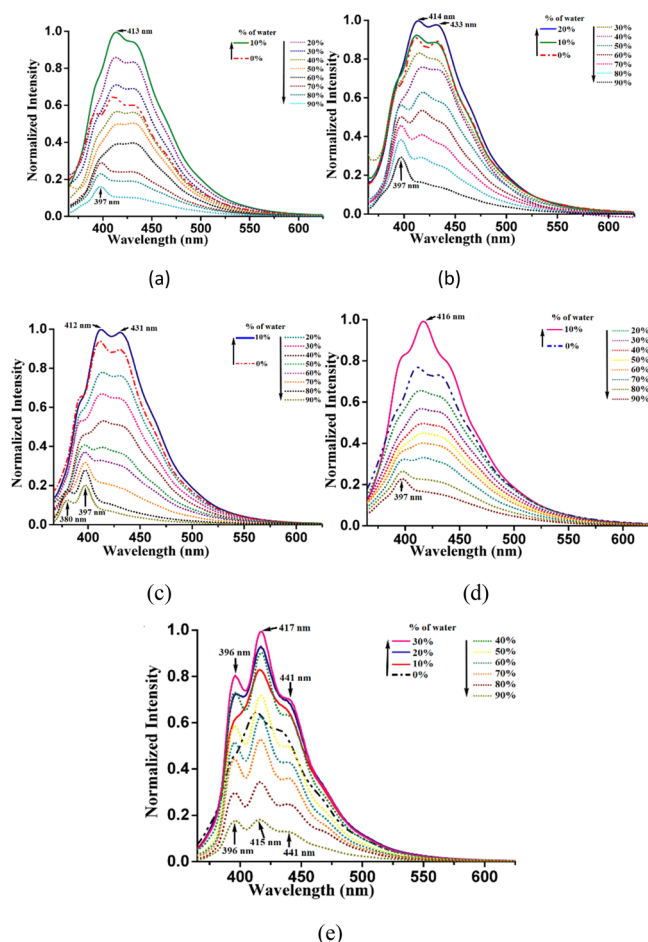


Figure 5. Fluorescence emission spectra ($\lambda_{\text{ex}} = 350 \text{ nm}$) of complexes (a) 1, (b) 2, (c) 3, (d) 4, and (e) 5 (each complex is 10^{-4} M in dimethyl sulfoxide) upon addition of different amounts of water (thick lines show an initial increase, whereas dotted lines show a decrease in emission).

emissions to study the enhancement and decrease due to aggregation. Since the HOMOs are associated with the metal part and the LUMOs are ligand-centric, it may be suggested that charge-transfer emission of these complexes could be modulated through aggregation.

The complexes remain as aggregates in solution and changes with the concentration of water, which are reflected in the dynamic light scattering studies enlisted in Figures S21–S24. The complex 1 dissolved in DMSO shows an average particle

size of 577.7 nm, and the same complex in DMSO having 50% water has an average particle size of 765.3 nm. This shows an increase in the size of the particles of the aggregate upon addition of water. This is also the case found in the other examples listed in Table 2. Complexes 1 and 2 have clear unimodal aggregation. Complex 3 has three different sets of aggregates, which convert to one set upon dilution. Dilution caused segregation of particles in the case of complex 4 to form two independent aggregates. The photoluminescence decay profile in solution was determined for each complex dissolved in DMSO and DMSO containing 50% water. It is observed that, in each case, there is a biexponential path. Each complex dissolved in dimethyl sulfoxide shows that a major fraction follows emission decay through a shorter lifetime of less than 1 ns, whereas a minor portion of the complexes passes through a relatively longer lifetime ranging between 4.9 and 6.9 ns. The trend changes on addition of 10% water; in such a situation, a higher fraction follows a relatively longer lifetime path (Table 2). These indicate that water-assisted aggregation formed initially (revealed in the DLS study) caused enhancement to follow a higher lifetime emission path.

The energies of the four non-ionic forms of complexes 1–4 are optimized by DFT calculation Figure 6. Each synthesized complex is taken as a reference to form different combinations as shown in Figure 6, which are taken up for energy calculations. Complexes 1a, 1b, and 1c have energy differences from the energy of complex 1 as +52.8820, -3.1285 , and $+76.1563 \text{ kJ/mol}$, respectively. Similarly, energy differences of the respective complexes 2a, 2b, and 2c are -37.0616 , -37.0437 , and $+34.5274 \text{ kJ/mol}$, respectively, from the energy of complex 2. The energy differences of complexes 3a, 3b, and 3c are $+104.0622$, -80.3414 , and $+61.4571 \text{ kJ/mol}$, respectively, from the energy of complex 3, whereas complexes 4a, 4b, and 4c have energy differences of -51.2910 , $+16.3595$, and $+48.9086 \text{ kJ/mol}$, respectively, from complex 4. Hence, the experimentally observed complexes except complex 3 are not the one that has the lowest energy among the different forms that are formulated in each case for the purpose of comparison. The observed complexes in the three cases are not the least stable one among them. These complexes with a dimeric structure as that of complex 3 have the lowest HOMO–LUMO energy gaps. For example, HOMO–LUMO energy gaps for the S_1 to S_0 transition are 3.7799 eV (328.01 nm) for 3, 3.2623 eV (380.05 nm) for 3a, 3.7342 eV (332.02 nm) for 3b, and 3.0820 eV (402.28 nm) for 3c. HOMO–LUMO gaps are 4.1367 eV (299.72 nm) for complex 1, 3.2623 eV (380.05 nm) complex 1a, 4.2096 eV (294.53 nm) complex

Table 2. Average Particle Size Determined by Dynamic Light Scattering, Quantum Yields, and Emission Lifetime

complex	in DMSO		quantum yield in DMSO (in DMSO + 10% H_2O) ^a	in DMSO with 50% water		in DMSO		in DMSO with 50% water	
	average particle size (nm)	polydispersity		average particle size (nm)	polydispersity	emission lifetime in ns (fraction %)			
1	577.7	0.284	0.0052 (0.108)	765.3	0.239	0.96 (88.80); 4.90 (12.20)			
2	296.3	0.441	0.0160 (0.0188)	570.0	0.240	0.98 (86.87); 6.87 (13.25)			
3	240.9	0.724	0.0136 (0.0189)	701.79	0.266	0.98 (87.78); 6.04 (12.22)			
4	125.0	0.441	0.0113 (0.1089)	409.7	0.793	0.94 (87.85); 5.29 (12.15)			
						0.96 (64.77); 6.23 (35.23)			
						0.93 (76.10); 5.95 (23.90)			
						0.99 (55.64); 5.53 (44.36)			
						0.90 (82.05); 6.15 (17.95)			

^aWith respect to quinone sulfate.

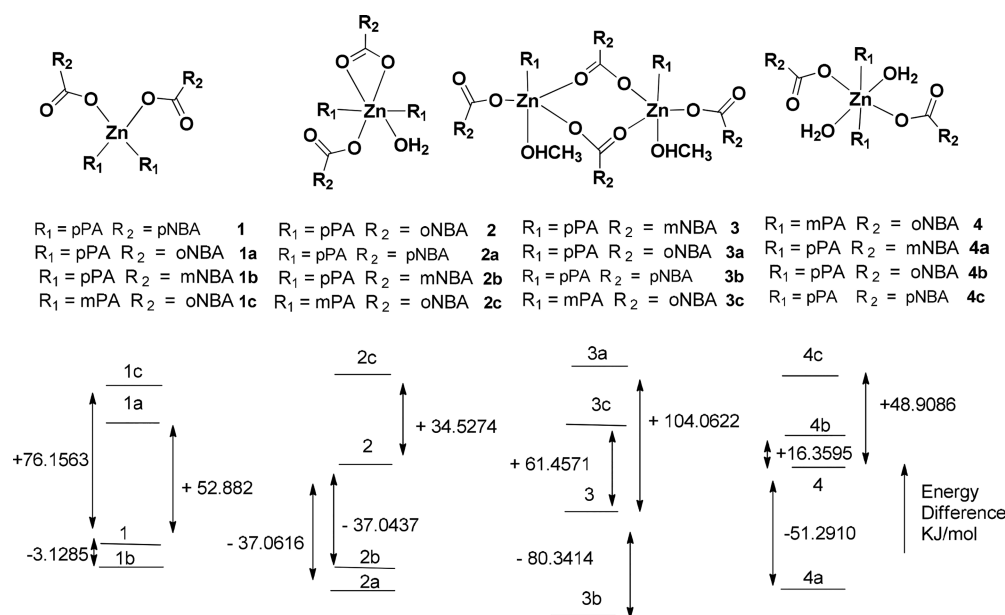
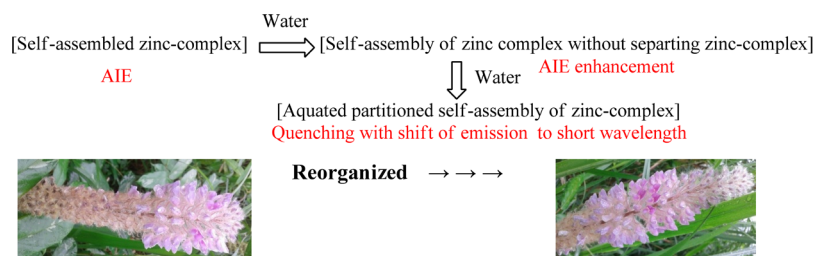


Figure 6. Comparative energy of different non-ionic complexes with respect to an experimentally observed structure calculated by DFT using the B3LYP functional with LANL2DZ as a basis set.

Scheme 2. Water-Assisted Reorganized Self-Assemblies^a



^aAt the bottom are two photos of two flowers called Asian foxtail (scientific name *Uraria crinita*) to show that aggregated floral parts may be distributed differently showing similar aesthetic sense.

1b, and 3.7654 eV (329.27 nm) for complex **1c**. Similar gaps for complexes **2**, **2a**, **2b**, and **2c** are 334.22, 303.11, 297.12, and 324.71 nm, respectively. On the other hand, gaps for the complexes with pyridine-3-carboxamide **4**, **4a**, **4b**, and **4c** are 317.13, 289.49, 318.36, and 296.56 nm, respectively. Similarly, for complex **5**, the cationic parts of positional isomeric complexes listed in Supporting Figure S30 are optimized. The energy gaps of the cations are found to be between 274.63 and 316.02 nm. The observed emission for the complex **5** was at 448 nm, which is a much longer wavelength from the anticipated S_1 to S_0 transition.

These results have shown that the emission in solution occurs at a higher wavelength than the theoretically calculated S_1 – S_0 transition. Furthermore, the increase in the concentration of water initially competes with the solvent to make an organized structure by taking possible coordination sites and making an assembly suitable for showing AIE. As the amount of water increases, water reorganizes the assembly to segregate the self-assembled zinc complexes yet provides scope to remain as newly formed assemblies through fast exchange that are not detected in the NMR time scale in solution.³⁷ Such equilibria are possible as the change of solvents makes different zinc complexes²⁷ and dimensionality of carboxylate polymers changes with solvent coordination.⁵⁶ The changes in dimensionality also affect the photoluminescence properties.⁶³

Water helping to construct self-assembly among the complexes at a low concentration caused an increase in intensity of emission followed by the decrease in emission intensity with wavelength shift due to disruptions. These occurred due to equilibrium between self-assemblies and lower nuclearity hydrated species as illustrated in Scheme 2. We have studied the ¹H NMR titrations on possible exchanges of ligands by externally adding different positional isomers of the pyridine-carboxamide to solution of the individual complex. There was no exchange of ligands as the spectra remained unchanged, showing inability to detect the exchange at the NMR time scale.

CONCLUSIONS

This study provides information on the various zinc complexes formed from different positional isomers and unfolds significance of the complex composed of nonfluorescent ligands to act as AIEgens in solid and solution. Irrespective of structures adopted by the zinc complexes derived from those positional isomers of nitrobenzoate and pyridinecarboxamide, each shows aggregation-induced emission. The amounts of water needed in solution for each complex to cause maximum emission intensity varied from complex to complex. In solution, complexes **1**–**5** showing emission enhancement without a shift in wavelength of emission upon addition of

water are indicative of the formation of a suitable assembly for aggregation-induced emission with assistance of water. It is likely to favor intermolecular self-assembly among zinc complexes at a lower water content. As the concentration of water increases, participation of water molecules in the formation of hydrogen bonds to reconstruct or reorganize the self-assemblies of the complexes results in quenching of emissions with a shift of emission to a shorter wavelength. A theoretical study has suggested that the wavelengths of emission of these complexes with or without adding water do not commensurate the calculated band gaps for the S_1 to S_0 transition. The complexes upon addition of excess water have emissions that are close to the emission calculated for a dimeric structure, showing disintegration of self-assemblies among the complex by excess water. The theoretically calculated HOMO–LUMO gaps of the four non-ionic forms suggest that the dinuclear carboxylate-bridged zinc complexes formulated with a skeleton of complex **3** with different positional isomers have the least energies relative to the ones formulated as mononuclear complexes.

EXPERIMENTAL SECTION

Physical Measurements. Infrared spectra of the solid samples were recorded on a Perkin-Elmer Spectrum-One FT-IR spectrophotometer by making KBr pellets. Powder X-ray diffraction patterns were recorded using a Bruker powder X-ray diffractometer D2 phaser. ^1H NMR spectra of complexes were recorded on a BRUKER Ascend-600 MHz NMR spectrometer using TMS as an internal standard. Elemental analyses were done on a EuroEA elemental analyzer. Fluorescence emissions were measured in a Horiba Jobin Yvon Fluoromax-4 spectrofluorometer by taking definite amounts of solutions or definite amounts of solid samples and exciting at a required wavelength. Quantum yields of the solid samples were measured by taking a definite amount of the solid and exciting at a required wavelength in a Horiba Jobin Yvon Fluoromax-4 spectrofluorometer using the Petite Integrating Sphere method. The fluorescence emission (E_c) and the scatter (L_c) for the sample and a blank (L_a and E_a) were recorded. From these spectral measurements (sample and blank), the quantum yields were calculated by using the equation $\varphi_F = [(E_c - E_a)/L_a - L_c]$. The radiationless (k_{nr}) and radiative rate constants (k_r) are calculated by using the formulas $k_{nr} = (1 - \Phi_F)/\tau$ and $k_r = \Phi_F/\tau$, where τ is the experimentally determined lifetime of fluorescence decay.⁶⁴

The average particle sizes were determined by dynamic light scattering carried out on a Malvern Zeta Sizer Nano ZS instrument equipped with a 4.0 mW He-Ne laser operating at 633 nm. The DFT and TD-DFT calculations for complexes were carried out by using Gaussian 09W-64 1995–2013 using the B3LYP functional with LANL2DZ as a basis set, whereas complex **5** and the corresponding positional isomeric complexes based on this complex are calculated as mono-cationic species.

Synthesis and Characterization. *Bis(pyridine-4-carboxamide)di(4-nitrobenzoato)zinc(II)-Methanol (1)*. To a well stirred solution of pyridine-4-carboxamide (161.21 mg, 1.32 mmol) and 4-nitrobenzoic acid (334.24 mg, 2.0 mmol) in methanol, zinc(II) acetate dihydrate (219.51 mg, 1 mmol) was added. The resulting solution was stirred for about 3 h. A dirty white precipitate was formed, which was dissolved in water, and the resulting solution was kept undisturbed for crystallization (isolated yield: 61%). Elemental anal. calcd for

$\text{C}_{28}\text{H}_{28}\text{N}_6\text{O}_{12}\text{Zn}$: C, 47.59; H, 3.96; N, 11.89; found C, 47.20; H, 4.11; N, 11.81. ^1H NMR (600 MHz, DMSO- d_6): 8.74 (s, 4H), 8.27 (m, 4H), 8.16 (d, $J = 12$ Hz, 4H), 7.77 (m, 8H). IR (KBr, cm^{-1}): 3443 (w), 3370 (m), 3156 (m), 1695 (m), 1602 (m), 1408 (s), 1341 (s), 1157 (m), 1106 (m), 1027 (s), 951 (m), 858 (m), 799 (s), 716 (s), 644 (m), 616 (w), 536 (w), 481 (s).

Bis(pyridine-4-carboxamide)(aqua)di(2-nitrobenzoato)zinc(II) (2). Complex **2** was synthesized by an identical procedure as that of complex **1**, but 2NBA was used instead of 4NBA (isolated yield: 62%). Elemental anal. calcd for $\text{C}_{26}\text{H}_{22}\text{N}_6\text{O}_{11}\text{Zn}$: C, 47.28; H, 3.33; N, 12.73; found H, 3.36; N, 12.89. ^1H NMR (600 MHz, DMSO- d_6): 8.70 (d, $J = 6$ Hz, 4H), 8.31 (s, 4H), 7.77 (m, $J = 6$ Hz, 4H), 7.75 (m, $J = 6$ Hz, 4H), 7.66 (t, $J = 6$ Hz, 2H), 7.60 (t, $J = 6$ Hz, 2H). ^{13}C NMR (100 MHz, DMSO- d_6): 168.94, 166.79, 150.36, 149.24, 141.61, 132.30, 131.72, 130.68, 130.28, 123.00, 121.74 ppm. IR (KBr, cm^{-1}): 3392 (br, w), 1690 (m), 1613 (s), 1523 (s), 1481 (w), 1384 (s), 1224 (w), 1147 (m), 1072 (w), 1018 (m), 860 (s), 786 (m), 740 (m), 701 (m), 641 (s), 573 (w), 436 (s).

Di- μ^2 -(3-nitrobenzoato)[(methanol)(pyridine-3-carboxamide)(3-nitrobenzoato)zinc(II)] (3). Complex **3** was synthesized by the procedure followed for complex **1**, but 3NBA was used in lieu of 2NBA (isolated yield of the crystalline product: 60%). Elemental anal. calcd for $\text{C}_{42}\text{H}_{36}\text{N}_8\text{O}_{20}\text{Zn}_2$: C, 45.67; H, 3.26; N, 10.15; found C, 45.88; H, 3.31; N, 10.76. ^1H NMR (600 MHz, DMSO- d_6): 8.73 (s, 4H), 8.66 (s, 4H), 8.35 (d, $J = 6$ Hz, 8H), 8.29 (s, 4H), 7.78 (d, $J = 6$ Hz, 4H), 7.74 (s, 4H), 4.21 (s, 2H), 3.16 (s, 6H). ^{13}C NMR (100 MHz, DMSO- d_6): 169.34, 166.67, 150.49, 147.93, 141.80, 137.03, 136.00, 130.18, 125.91, 124.11, 121.87, 48.92 ppm. IR (KBr, cm^{-1}): 3582 (w), 3465 (w), 3409 (w), 3317 (w), 3078 (m), 2856 (w), 1953 (w), 1687 (s), 1612 (s), 1561 (w), 1525 (w), 1475 (w), 1393 (m), 1349 (m), 1225 (w), 1154 (m), 1071 (s), 1026 (s), 913 (s), 833 (s), 787 (s), 720 (s), 633 (s), 525 (m), 430 (m).

(Di-aqua)bis(pyridine-3-carboxamide)di(2-nitrobenzoato)zinc(II) monohydrate (4). To a well stirred solution of pyridine-3-carboxamide (161.19 mg, 1.32 mmol) and 2-nitrobenzoic acid (334.24 mg, 2.0 mmol) in ethanol, zinc(II) acetate dihydrate (219.51 mg, 1 mmol) was added. The resulting solution was stirred for about 3 h. The precipitate formed was dissolved in water, and the resulting solution was kept undisturbed for crystallization (isolated yield: 60%). Elemental anal. calcd for $\text{C}_{26}\text{H}_{28}\text{N}_6\text{O}_{14}\text{Zn}$: C, 43.70; H, 3.92; N, 11.76; found C, 43.28; H, 3.97; N, 11.21. ^1H NMR (600 MHz, DMSO- d_6): 9.02 (s, 2H), 8.70 (m, 2H), 8.21 (m, 4H), 7.80 (m, $J = 6$ Hz, 4H), 7.66 (s, 2H), 7.61 (m, 4H), 7.51 (m, $J = 6$ Hz, 2H). ^{13}C NMR (100 MHz, DMSO- d_6): 166.75, 152.21, 150.10, 149.57, 148.97, 135.50, 135.36, 132.29, 130.52, 129.98, 123.76, 123.11 ppm. IR (KBr, cm^{-1}): 3388 (m), 3154 (m), 1681 (s), 1601 (s), 1534 (s), 1440 (w), 1381 (s), 1197 (w), 1136 (s), 1054 (w), 970 (w), 859 (w), 776 (s), 739 (m), 695 (s), 650 (s), 538 (w), 426 (s).

[Tri-aqua(pyridine-3-carboxamide)(κ -O- κ -O'-4-nitrobenzoato)zinc(II)]4-nitrobenzoate (5). Zinc complex **5** was synthesized by an identical procedure as that of complex **4**, and 4NBA was used instead of 2NBA. The precipitate was dissolved in water, and the resulting solution was kept undisturbed for crystallization (isolated yield: 62%). Elemental anal. calcd for $\text{C}_{20}\text{H}_{20}\text{N}_4\text{O}_{12}\text{Zn}$: calcd. C, 41.82; H, 3.49; N, 9.76; found C, 41.96; H, 3.58; N, 9.51. ^1H NMR (600 MHz,

DMSO- d_6): 9.03 (s, 1H), 8.70 (m, 1H), 8.27 (m, $J = 6$ Hz, 4H), 8.21 (m, $J = 12$ Hz, 2H), 8.16 (m, $J = 6$ Hz, 4H), 7.63 (s, 1H), 7.51 (m, $J = 6$ Hz, 1H). ^{13}C NMR (100 MHz, DMSO- d_6) 169.60, 166.76, 152.21, 149.33, 148.98, 141.15, 135.57, 131.04, 130.03, 123.81, 123.59 ppm. IR (KBr, cm^{-1}): 3556 (m), 3428 (w), 3364 (w), 3319 (w), 3277 (w), 3230 (w), 3115 (w), 2926 (w), 1952 (m), 1680 (s), 1609 (m), 1558 (s), 1427 (m), 1382 (m), 1345 (s), 1206 (w), 1158 (m), 1105 (s), 1062 (s), 1011 (m), 875 (s), 845 (m), 802 (s), 751 (w), 724 (s), 685 (w), 630 (m), 520 (s).

■ ASSOCIATED CONTENT


Supporting Information

The Supporting Information is available free of charge at <https://pubs.acs.org/doi/10.1021/acsomega.0c00136>.

^1H NMR, ^{13}C NMR, powder X-ray diffraction patterns, fluorescence lifetime decay profiles, dynamic light scattering profiles, and theoretically determined HOMO–LUMO gaps of the model complexes (PDF)
X-ray crystallographic data of complex 4 (CIF)
X-ray crystallographic data of complex 5 (CIF)
X-ray crystallographic data of complex 2 (CIF)
X-ray crystallographic data of complex 3 (CIF)
X-ray crystallographic data of complex 1 (CIF)

■ AUTHOR INFORMATION

Corresponding Author

Jubaraj B. Baruah – Department of Chemistry, Indian Institute of Technology Guwahati, Guwahati 781 039, Assam, India;
 orcid.org/0000-0003-3371-7529; Email: juba@iitg.ac.in

Author

Rinki Brahma – Department of Chemistry, Indian Institute of Technology Guwahati, Guwahati 781 039, Assam, India

Complete contact information is available at:

<https://pubs.acs.org/doi/10.1021/acsomega.0c00136>

Notes

The authors declare no competing financial interest.
The CCDC nos. for the crystallographic information files of complexes 1–5 deposited in the Cambridge Crystallographic Database are 1964039–1964043.

■ ACKNOWLEDGMENTS

The authors thank the Ministry of Human Resources and Development, New-Delhi, India, for financial assistance through departmental grant No. F. No. 5-1/2014-TS.VII.

■ REFERENCES

- (1) Holub, J.; Santoro, A.; Lehn, J.-M. Electronic absorption and emission properties of bishydrazone $[2 \times 2]$ metallosupramolecular grid-type architectures. *Inorg. Chim. Acta* **2019**, *494*, 223–231.
- (2) Chen, Y.; Bai, Y.; Han, Z.; He, W.; Guo, Z. Photoluminescence imaging of Zn^{2+} in living systems. *Chem. Soc. Rev.* **2015**, *44*, 4517–4546.
- (3) Borbone, F.; Caruso, U.; Concilio, S.; Nabha, S.; Panunzi, B.; Piotto, S.; Shikler, R.; Tuzi, A. Mono-, di-, and polymeric pyridinoylhydrazone Zn^{II} complexes: structure and photoluminescent properties. *Eur. J. Inorg. Chem.* **2016**, 818–825.
- (4) Diana, R.; Panunzi, B.; Tuzi, A.; Caruso, U. Two tridentate pyridinyl-hydrazone zinc(II) complexes as fluorophores for blue emitting layers. *J. Mol. Struct.* **2019**, *1197*, 672–680.

(5) Xu, Z.; Baek, K.-H.; Kim, H. N.; Cui, J.; Qian, X.; Spring, D. R.; Shin, I.; Yoon, J. Zn^{2+} -triggered amide tautomerization produces a highly Zn^{2+} -selective, cell-permeable, and ratiometric fluorescent sensor. *J. Am. Chem. Soc.* **2010**, *132*, 601–610.

(6) Liang, L. J.; Zhao, X. J.; Huang, C. Z. $\text{Zn}(\text{II})$ complex of terpyridine for the highly selective fluorescent recognition of pyrophosphate. *Analyst* **2012**, *137*, 953–958.

(7) Zheng, S.-L.; Yang, J.-H.; Yu, X.-L.; Chen, X.-M.; Wong, W.-T. Syntheses, structures, photoluminescence, and theoretical studies of d^{10} metal complexes of 2,2'-Dihydroxy-[1,1']binaphthalenyl-3,3'-dicarboxylate. *Inorg. Chem.* **2004**, *43*, 830–838.

(8) Dey, S.; Efimov, A.; Giri, C.; Rissanen, K.; Lemmetyinen, H. Electronic structure manipulation of (benzothiazole) zinc complexes: Synthesis, optical and electrochemical studies of 5-substituted derivatives. *Eur. J. Org. Chem.* **2011**, 6226–6232.

(9) Dumur, F. Zinc complexes in OLEDs: an overview. *Synth. Met.* **2014**, *195*, 241–251.

(10) Kim, D.-E.; Shin, H.-K.; Kim, N.-K.; Lee, B.-J.; Kwon, Y.-S. White organic light-emitting diodes with Zn-complexes. *J. Nanosci. Nanotechnol.* **2014**, *14*, 1019–1032.

(11) Nishal, V.; Singh, D.; Saini, R. K.; Bhagwan, S.; Tanwar, V.; Sonika, S.; Srivastava, R.; Kadyan, P. S. Optoelectronic characterization of zinc complexes for display device applications. *J. Mater. Sci.: Mater. Electron.* **2015**, *26*, 6762–6768.

(12) Ma, R.; Schuette, G. F.; Broadbelt, L. J. Microkinetic modeling of CO_2 hydrolysis over Zn -(1,4,7,10-tetraazacyclododecane) catalyst based on first principles: revelation of rate-determining step. *J. Catal.* **2014**, *317*, 176–184.

(13) Liu, X.; Du, P.; Cao, R. Trinuclear zinc complexes for biologically relevant μ^3 -oxoanion binding and carbon dioxide fixation. *Nat. Commun.* **2013**, *4*, 2375.

(14) Ohshima, T.; Iwasaki, T.; Mashima, K. Direct conversion of esters, lactones, and carboxylic acids to oxazolines catalyzed by a tetranuclear zinc cluster. *Chem. Commun.* **2006**, *37*, 2711–2713.

(15) Iwasaki, T.; Maegawa, Y.; Hayashi, Y.; Ohshima, T.; Mashima, K. Transesterification of various methyl esters under mild conditions catalyzed by tetranuclear zinc cluster. *J. Org. Chem.* **2008**, *73*, 5147–5150.

(16) Xia, J.; Xu, Y.; Li, S.-A.; Sun, W.-Y.; Yu, K.-B.; Tang, W.-X. Carboxy ester hydrolysis promoted by a zinc(II) 2-[bis(2-aminoethyl)amino]ethanol complex: a new model for indirect activation on the serine nucleophile by zinc(II) in zinc enzymes. *Inorg. Chem.* **2001**, *40*, 2394–2401.

(17) Gupta, A. K.; Dhir, A.; Pradeep, C. P. Multifunctional Zn(II) complexes: photophysical properties and catalytic transesterification toward biodiesel synthesis. *Inorg. Chem.* **2016**, *55*, 7492–7500.

(18) Kimura, E. Model studies for molecular recognition of carbonic anhydrase and carboxypeptidase. *Acc. Chem. Res.* **2001**, *34*, 171–179.

(19) Reger, D. L.; Debreczeni, A.; Smith, M. D. Homochiral, supramolecular frameworks built from a zinc(II) tetramer or cadmium(II) dimer containing enantiopure carboxylate ligands functionalized with a strong $\pi \cdots \pi$ stacking synthon. *Eur. J. Inorg. Chem.* **2012**, 712–719.

(20) Tao, J.; Shi, J.-X.; Tong, M.-L.; Zhang, X.-X.; Chen, X.-M. A new inorganic-organic photoluminescent material constructed with helical $[\text{Zn}_3(\mu^3\text{-OH})(\mu^2\text{-OH})]$ chains. *Inorg. Chem.* **2001**, *40*, 6328–6330.

(21) Khakhlary, P.; Baruah, J. B. Studies on cluster, salt and molecular complex of zinc-quinolate. *J. Chem. Sci.* **2015**, *127*, 215–223.

(22) Khajavi, H.; Gascon, J.; Schins, J. M.; Siebbeles, L. D. A.; Kapteijn, F. Unraveling the optoelectronic and photochemical behavior of Zn_4O -based metal organic frameworks. *J. Phys. Chem. C* **2011**, *115*, 12487–12493.

(23) Goswami, A.; Phukan, N.; Baruah, J. B. Tetranuclear zinc(II)-oxy (benzothiazole)-2-thiolate aggregate and copper(I) phenylthiolate aggregate. *Cogent Chem.* **2015**, *1*, 1060046.

(24) Bertinello, R.; Bettinelli, M.; Casarin, M.; Gulino, A.; Tondello, E.; Vittadini, A. Hexakis(acetato)oxotetrazinc, a well-

tailored molecular model of zinc oxide. An experimental and theoretical investigation of the electronic structure of $\text{Zn}_4\text{O}(\text{acetate})_6$ and ZnO by means of UV and x-ray photoelectron spectroscopies and first principle local density molecular cluster calculations. *Inorg. Chem.* **1992**, *31*, 1558–1565.

(25) Chun, H.; Jung, H. Targeted synthesis of a prototype MOF based on $\text{Zn}_4(\text{O})(\text{O}_2\text{C})_6$ units and a nonlinear dicarboxylate ligand. *Inorg. Chem.* **2009**, *48*, 417–419.

(26) Sarma, R.; Kalita, D.; Baruah, J. B. Solvent induced reactivity of 3, 5-dimethylpyrazole towards zinc (II) carboxylates. *Dalton Trans.* **2009**, 7428–7436.

(27) Karmakar, A.; Baruah, J. B. Synthesis and characterization of zinc benzoate complexes through combined solid and solution phase reactions. *Polyhedron* **2008**, *27*, 3409–3416.

(28) Trosch, A.; Vahrenkamp, H. A sterically hindered N,N,O tripod ligand and its zinc complex chemistry. *Inorg. Chem.* **2001**, *40*, 2305–2311.

(29) Bhattacharyya, S.; Kumar, S. B.; Dutta, S. K.; Tiekink, E. R. T.; Chaudhury, M. Zinc(II) and copper(II) complexes of pentacoordinating (N_4S) ligands with flexible pyrazolyl arms: syntheses, structure, and redox and spectroscopic properties. *Inorg. Chem.* **1996**, *35*, 1967–1973.

(30) Kimura, E.; Kurosaki, H.; Koike, T.; Toriumi, K. X-ray structural study of a zinc(II) inclusion complex of a phenolate-pendant cyclam. *J. Inclusion Phenom. Mol. Recognit. Chem.* **1992**, *12*, 377–387.

(31) Kimura, E.; Koike, T. Macrocyclic polyamines as a probe for equilibrium study of the acid functions of zinc(II) ion in hydrolysis enzymes. *Comments Inorg. Chem.* **1991**, *11*, 285–301.

(32) Castro, J. A.; Romero, J.; Garcia-Vazquez, J. A.; Macias, A.; Sousa, A.; Englert, U. Electrochemical synthesis of metal(II) complexes of Schiff bases: the crystal structure of acetonitrile-bis{2-[(2-pyrrolo)methylimino]-4,6-dimethylphenolato}zinc(II). *Polyhedron* **1993**, *12*, 1391–1397.

(33) Rivas, J. C. M.; Salvagni, E.; de Rosales, R. T. M.; Parsons, S. Internal hydrogen bonding in tetrahedral and trigonal bipyramidal zinc(II) complexes of pyridine-based ligands. *Dalton Trans.* **2003**, 3339–3349.

(34) Baruah, A. M.; Sarma, R.; Baruah, J. B. A penta-coordinated bis-(8-aminoquinoline) monobenzoato zinc(II) benzoate complex favored by self-assembly formation. *Inorg. Chem. Commun.* **2008**, *11*, 121–124.

(35) Choi, K.-Y. Synthesis and structural characterization of zinc(II) complexes of 2,5,9,12-tetramethyl-1,4,8,11-tetraazacyclotetradecane. *Polyhedron* **1998**, *17*, 1975–1982.

(36) Berezin, A. S.; Antonova, O. V.; Lider, E. V.; Smolentsev, A. I.; Nadolinny, V. A.; Mel'gunov, M. S. Sample-size dependence of the fluorescence of 2-(N-acetylamino)-6-methylpyridine and its zinc(II) chloride complex. *J. Lumin.* **2017**, *190*, 261–266.

(37) Nath, J.; Tarai, A.; Baruah, J. B. Copper (II), Zinc (II), and Cadmium (II) Formylbenzoate complexes: reactivity and emission properties. *ACS Omega* **2019**, *4*, 18444–18455.

(38) Evans, D. A.; Lee, L. M.; Vargas-Baca, I.; Cowley, A. H. Photophysical tuning of the aggregation-induced emission of a series of *para*-substituted aryl bis(imino)acenaphthene zinc complexes. *Dalton Trans.* **2015**, *44*, 11984–11996.

(39) Qiao, D.; Wang, J.-Y.; Zhang, L.-Y.; Dai, F.-R.; Chen, Z.-N. Aggregation-induced emission enhancement and reversible mechanochromic luminescence of quinoline-based zinc(II)–Schiff base complexes. *Dalton Trans.* **2019**, *48*, 11045–11051.

(40) Evans, D. A.; Lee, L. M.; Vargas-Baca, I.; Cowley, A. H. Aggregation-induced emission of bis(imino)acenaphthene zinc complexes: photophysical tuning via methylation of the flanking aryl substituents. *Organometallics* **2015**, *34*, 2422–2428.

(41) Xie, Y.-Z.; Shan, G.-G.; Li, P.; Zhou, Z.-Y.; Su, Z.-M. A novel class of Zn(II) Schiff base complexes with aggregation-induced emission enhancement (AIEE) properties: Synthesis, characterization and photophysical/electrochemical properties. *Dyes Pigm.* **2013**, *96*, 467–474.

(42) Xiong, J.; Wang, K.; Yao, Z.; Zou, B.; Xu, J.; Bu, X.-H. Multi-stimuli-responsive fluorescence switching from a pyridine-functionalized tetraphenylethene AIEgen. *ACS Appl. Mater. Interfaces* **2018**, *10*, 5819–5827.

(43) Xiong, J.; Li, X.; Yuan, C.; Semin, S.; Yao, Z.; Xu, J.; Rasing, T.; Bu, X.-H. Wavelength dependent nonlinear optical response of tetraphenylethene aggregation-induced emission luminogens. *Mater. Chem. Front.* **2018**, *2*, 2263–2271.

(44) Luo, J.; Xie, Z.; Lam, J. W. Y.; Cheng, L.; Chen, H.; Qiu, C.; Kwok, H. S.; Zhan, X.; Liu, Y.; Zhu, D.; Tang, B. Z. Aggregation-induced emission of 1-methyl-1,2,3,4,5-pentaphenylsilole. *Chem. Commun.* **2001**, 1740–1741.

(45) Mei, J.; Leung, N. L. C.; Kwok, R. T. K.; Lam, J. W. Y.; Tang, B. Z. Aggregation-induced emission: together we shine, united we soar! *Chem. Rev.* **2015**, *115*, 11718–11940.

(46) Hong, Y.; Lam, J. W. Y.; Tang, B. Z. Aggregation-induced emission. *Chem. Soc. Rev.* **2011**, *40*, 5361–5388.

(47) Baruah, A. M.; Karmakar, A.; Baruah, J. B. Steric effects in controlling co-ordination environment in zinc 2-nitrobenzoate complexes. *Inorg. Chim. Acta* **2008**, *361*, 2777–2784.

(48) Bujdošová, Z.; Györyová, K.; Růžička, A.; Melník, M.; Koman, M. Crystal structures of two aromatic zinc(II) carboxylates: $[\text{Zn}(4\text{-chlorosalicylate})_2(\text{H}_2\text{O})_4]\cdot 2\text{theophylline}\cdot(\text{H}_2\text{O})_2$ and unique $[\text{Zn}(5\text{-chlorosalicylate})_2(\text{isonicotinamide})_2(\text{H}_2\text{O})]$. *J. Chem. Crystallogr.* **2011**, *41*, 1077–1084.

(49) Homzová, K.; Györyová, K.; Koman, M.; Melník, M.; Juhászová, Z. Synthesis, crystal structure, and spectroscopic and thermal properties of the polymeric compound *catena*-poly[[*bis*(2,4-dichlorobenzoato)zinc(II)]- μ -isonicotinamide]. *Acta Crystallogr.* **2015**, *71*, 814.

(50) Findoráková, L.; Györyová, K.; Koman, M.; Moncol, J.; Melník, M. Crystal structure and physical characterisation of $[\text{Zn}_2(\text{Benzoato})_4(\text{Caffeine})_2]\cdot 2\text{Caffeine}$. *J. Chem. Crystallogr.* **2010**, *40*, 145–150.

(51) Lin, J.-G.; Qiu, L.; Cheng, W.; Luo, S.-N.; Wang, K.; Meng, Q.-J. A novel cobalt(II) complex based on nicotinamide and 2-nitrobenzoate mixed ligands: Synthesis, characterization, and biological activity. *Inorg. Chem. Commun.* **2010**, *13*, 855–858.

(52) Bozkurt, E.; Çelik, Y.; Çöpür, F.; Dege, N.; Topcu, Y.; Karabulut, B. Synthesis, crystal structure and EPR studies of vanadyl doped $[\text{Co}(2\text{-nbH})_2(\text{ina})_2(\text{H}_2\text{O})]$ complex. *Chem. Phys. Lett.* **2016**, *659*, 186–191.

(53) Stachová, P.; Melník, M.; Korabik, M.; Mrozinski, J.; Koman, M.; Glowiak, T.; Valigura, D. Synthesis, spectral and magnetical characterization of monomeric $[\text{Cu}(2\text{-NO}_2\text{bz})_2(\text{nia})_2(\text{H}_2\text{O})_2]$ and structural analysis of similar $[\text{Cu}(\text{RCOO})_2(\text{L}-\text{N})_2(\text{H}_2\text{O})_2]$ complexes. *Inorg. Chim. Acta* **2007**, *360*, 1517–1522.

(54) Karmakar, A.; Bania, K.; Baruah, A. M.; Baruah, J. B. Role of nitro-substituent in pseudo-polymorphism and in synthesis of metal carboxylate complexes of copper, zinc and manganese. *Inorg. Chem. Commun.* **2007**, *10*, 959–964.

(55) Karmakar, A.; Sarma, R. J.; Baruah, J. B. Self-assembly of neutral dinuclear and trinuclear zinc-benzoate complexes. *Inorg. Chem. Commun.* **2006**, *9*, 1169–1172.

(56) Singh, W. M.; Baruah, J. B. Coordination polymers of zinc with 2,2'-(2,3-bis-phenylsulfanylnaphthalene-1,4-xyloxy)diacetic acid. *Dalton Trans.* **2009**, 2352–2358.

(57) Barboza, C. A.; Germino, J. C.; Santana, A. M.; Quites, F. J.; Vazquez, P. A. M.; Atvars, T. D. Z. Structural correlations between luminescent properties and excited state internal proton transfer in some zinc(II) N,N'-bis(salicylidenes). *J. Phys. Chem. C* **2015**, *119*, 6152–6163.

(58) Terenzi, A.; Lauria, A.; Almerico, A. M.; Barone, G. Zinc complexes as fluorescent chemosensors for nucleic acids: new perspectives for a “boring” element. *Dalton Trans.* **2015**, *44*, 3527–3535.

(59) Salassa, G.; Coenen, M. J. J.; Wezenberg, S. J.; Hendriksen, B. L. M.; Speller, S.; Elemans, J. A. A. W.; Kleij, A. W. Extremely strong

self-Assembly of a bimetallic salen complex visualized at the single-molecule level. *J. Am. Chem. Soc.* **2012**, *134*, 7186–7192.

(60) Le Bras, L.; Chaitou, K.; Aloise, S.; Adamo, C.; Perrier, A. Aggregation-caused quenching versus crystallization induced emission in thiazolo[5,4-*b*]thieno[3,2-*e*]pyridine (TTP) derivatives: theoretical insights. *Phys. Chem. Chem. Phys.* **2019**, *21*, 46–56.

(61) Christianson, D. W.; Alexander, R. S. Carboxylate-histidine-zinc interactions in protein structure and function. *J. Am. Chem. Soc.* **1989**, *111*, 6412–6419.

(62) Katiyar, A.; Sovierzoski, J. C. F.; Calio, P. B.; Vartia, A. A.; Thompson, W. H. Water plays a diverse role in a hydrogen-bonded, hexameric supramolecular assembly. *Chem. Commun.* **2019**, *55*, 6591–6594.

(63) Liu, B.; Pang, L.-Y.; Hou, L.; Wang, Y.-Y.; Zhang, Y.; Shi, Q.-Z. Two solvent-dependent zinc(II) supramolecular isomers: structure analysis, reversible and nonreversible crystal-to-crystal transformation, highly selective CO₂ gas adsorption, and photoluminescence behaviors. *CrystEngComm* **2012**, *14*, 6246–6251.

(64) Kapturkiewicz, A.; Herbich, J.; Karpiuk, J.; Nowacki, J. Intramolecular radiative and radiationless charge recombination processes in donor-acceptor carbazole derivatives. *J. Phys. Chem. A* **1997**, *101*, 2332–2344.